`Vol. 5, No. 3, pp. 229-242, (September 2024)
DOI: 10.21608/aujes.2024.299836.1258
Aswan University Journal of Environmental Studies (AUJES)
Online ISSN: 2735-4237, Print ISSN: 2735-4229
Journal homepage: https://aujes.journals.ekb.eg/ E-mail: AUJES@aswu.edu.eg
Original research

The effect of hydroxide anionic precursors on the anticancer activity of Zinc Oxide Nanoparticles Against Breast Cancer (MCF-7) Cell Line

Eman Hussien[1,2], Marwa A. Moghazy [2], Kh. Ebenlwaled[1] and Alaa Hassan Said[1,*]

[1] *Electronics and Nano Devices lab, Faculty of Science, South Valley University, Qena, Egypt.*
[2] *Environmental Applications of Nanomaterials Lab., Department of Chemistry, Faculty of Science, Aswan University, 81528 Aswan, Egypt.*

Received: 24/4/2024 Accepted: 6/9/2024

Abstract:

Zinc oxide nanoparticles (ZnO NPs) are a famous metal oxide, which is introduced in many daily life applications due to its physiochemical properties. Many parameters can influence the physiochemical properties of ZnO NPs such as pH, temperature, surface chemistry, solvent and precursors. In this work, we aim to investigate the role of hydroxide anionic precursors on the cytotoxicity of ZnO NPs against breast cancer. ZnO NPs were prepared by chemical precipitation using two different hydroxide anionic precursors (Ammonium hydroxide and Sodium hydroxide). X-ray diffraction (XRD) and High-Resolution Transmission Electron Microscope (HRTEM) were employed to study structural properties, while UV-visible spectroscopy was used for measuring the optical properties of the investigated samples. The induced toxic effect was screened using MTT cell proliferation assay. The obtained results confirmed the successful production of ZnO NPs from the two different anionic precursors (Sodium hydroxide and Ammonium hydroxide) using the chemical co-precipitation method. Structural analysis reveals that there is a direct effect of changing the hydroxide anionic precursors on the internal structure and particle size of ZnO NPs. The use of ammonium hydroxide as a hydroxide anionic precursor produces semispherical ZnO NPs with a larger particle size, higher crystallinity and smaller optical bandgap compared with sodium hydroxide. The anticancer activity was measured using MTT assay against breast cancer cells (MCF-7). The obtained results revealed that ZnO NPs synthesized using sodium hydroxide as an anionic hydroxide precursor have a higher activity than ZnO NPs synthesized using ammonium hydroxide.

Keywords: ZnO NPs, Breast cancer, MCF-7, cytotoxicity, sodium hydroxide.

1- Introduction

Cancer has been recognized as the second greatest cause of death worldwide, making it one of the most significant public health challenges. According to statistics, the number of monitored cases is constantly in the United States 1,762,450 new cancer cases and over 600,000 annual deaths were reported in 2019 **(Siegel et al., 2021)**.

Corresponding author*: E-mail address: alaa.elkareem@sci.svu.edu.eg

According to Global Cancer Observatory (GLOBOCAN) estimates, as of December 2020, the number of cancer cases in Egypt was 27,165 overall, with the most common cancers being breast (61,160), liver (28,977), bladder (26,986), lymphoma (19,096), leukemia (14,274), brain and central nervous system (11,470), and prostate (10,523) **(Ibrahim & Shash, 2022)**.

ZnO is a multifunctional nanomaterial possessing intriguing semiconducting properties. It characterizes by enormous band gap energy of 3.37 eV and strong excitation binding energy of 60 MeV**(Schumm, 2008)**. ZnO is a white powder and is insoluble in water and most ZnO used commercially is produced synthetically **(Bisht et al., 2016; Harun et al., 2016)**. Accordingly, ZnO NPs were introduced in many daily life applications due to their physiochemical properties. Many parameters can influence the physiochemical properties of ZnO NPs such as pH, temperature, surface chemistry, solvent and precursors. Depending on the NPs synthesis approaches, ZnO NPs can be obtained through three different routes: chemical, physical and biological routes. Chemical methods can be categorized according to the physical state to solid phase, liquid phase and vapor phase **(Król et al., 2017)**. Among these techniques are sol gel, hydrothermal, solvothermal, microwave, ultrasonic, plasma, electrochemical, and solid state **(Barhoum et al., 2018; Loganathan et al., 2021)**. Several factors can affect the precipitation of ZnO NPs including reaction pH, temperature and time. Moreover, Zn precursors such as zinc chloride, zinc sulphate and zinc acetate and solvent used can affect the size and morphology of the produced NPs. Precipitation techniques have been shown to have a number of benefits, including high quality and large-scale production of nanoscale materials without the requirement for hazardous organic solvents, as well as affordability and ease of use **(Limón- rocha et al., 2022)**.

ZnO NPs exhibit a high degree of selectivity towards a range of cancer cell types, including liver cancer cells (HepG2), epithelial cells (BEAS-2B), lung cancer cells (A549), human melanoma cells (A375), mouse melanoma cells (B16F10), human head and neck squamous cell (HNSCC), and breast cancer cell line MCF-7. These properties are attributed to ZnO NPs' unique intrinsic anticancer activity and ROS regeneration capability **(Ahmadi Shadmehri & Namvar, 2020; Bisht et al., 2016; Chung et al., 2015; Selvakumari et al., 2015)**. The smaller size of ZnO NPs facilities the internalization into the cellular membrane. Due to its high surface-to-volume ratio, it interacts with various biomolecules disrupting cellular homeostasis leading to apoptosis and cancer cell death **(Selvakumari et al., 2015)**.

Once ZnO NPs internalized into cancer cells, they ionized to zinc ions which initiate the ROS generation via cascaded reactions. In the culture media, the dissolved Zn ions interact and form poorly soluble amorphous zinc-carbonate phosphate precipitates. While inside the cell, the dissolved Zn ions increase the concentration of zinc ions which are already present inside the cell membrane leading to disturb the mediated protein activity equilibrium by oxidative stress which finally lead to cellular damage **(Król et al., 2017)**.

The smaller particle size as well as surface properties of ZnO NPs contribute to a very characteristic property, which is the permeation and retention effect (EPR) in tumor cells. Cancer cells are cells with uncontrolled growth therefore they have limited number of blood and lymphatic vessels and less cellular connections. Moreover, the blood contains many pores with different sizes ranging from 100 nm to 1 micrometer. These characteristics enhance the diffusion of NPs through the blood vessels to cancer cells showing enhanced permeation selectively. The localized NPs inside the cancer cells didn't move quickly by interstitial fluid surrounding the cell due to the improper lymphatic system of cancer cells and took longer retention time. With the

increasing permeation and retention process, the selectivity and efficacy of NPs to destroy the cancer cells increased **(Bisht et al., 2016; Nam et al., 2013)**. The electrostatic interaction between ZnO NPs and cancer cells is another factor that contributes to ZnO NPs' sensitivity to cancer cells. It's reported that ZnO NPs exhibit a positive charge in physiological medium, whereas cancer cells exhibit a negative charge as a result of the elevated levels of negatively charged anionic phospholipids on their surface. This causes ZnO NPs to be more attractive to cancer cells, which improves ZnO NP uptake and localization **(Fröhlich, 2012; Rasmussen et al., 2010)**.

The presented work motivates us to investigate the role of hydroxide anionic precursors on the cytotoxicity of ZnO NPs.

2. Materials and Methods

2.1 Materials

Materials used in this study were used without purification. Sodium hydroxide, Ammonium hydroxide and Zinc acetate dehydrate were purchased from (Oxford Company, India). 0.05% Trypsin-EDTA, Dulbecco's modified Eagle's medium (DMEM), Demso Phosphate buffered saline (PBS), Fetal bovine serum (FBS), penicillin/ streptomycin (P/S) and MTT (3-(4,5-dimethylthiazol-2-yl)-2,5-diphenyltetrazolium bromide) were purchased from (Himedia -India). Breast cancer cell line (MCF- 7) obtained from the Egyptian holding company for biological products and vaccines (Vacsera - Egypt). This work was approved by the Ethics Committee of South Valley University, Faculty of Science (Permit Number: 003/08/24).

2.2 ZnO NPs preparation from two hydroxide anionic precursors

The chemical precipitation method was adopted to synthesize ZnO NPs with two hydroxide anionic precursors (Sodium hydroxide and Ammonium hydroxide), Figure (1) **(Koutu et al., 2016)**. Briefly, Zinc acetate dehydrate (Zn $(CH_3COO)_2 \cdot 2H_2O$) was dissolved in 50 ml distilled water (D.W) under vigorous stirring at room temperature. Hydroxide anionic precursor (NaOH or NH_4OH) was added dropwise to adjust the pH to 12 under vigorous stirring for 2 hr. The following day, the precipitate was collected using centrifugation and properly cleaned three times using D.W. and once with ethanol to get rid of any remaining residues then dried at 100 ºC.

2.3 Characterization of ZnO NPs

X'Pert PRO-PAN diffractometer with Cu-Kα radiation (λ= 1.54056 A˚) was used for phase identification and structural analysis of the investigated samples. A high-resolution Transmission electron microscope (**JEOL, JEM 2100, Japan**) was used for further morphological and structural studies. Optical absorption of the investigated samples was recorded using UV-visible spectrophotometer (**SPECORD 200 PLUS, Analytik Jena, Germany**).

2.4 Cytotoxicity of ZnO NPs synthesized using two hydroxide anionic precursors

Human breast cancer cell lines (MCF-7) were used to evaluate the cytotoxicity of the prepared samples. Complete culture media was prepared using DMEM containing 4.5 g/l, Glucose with L-Glutamine, 10 % heat-inactivated FBS and 1 % P/S. Cells with density 1×10^5 cell/well were cultured in 96 well plate and incubated at 37°C, 5% CO_2 for 24h. ZnO NPs solution was prepared by dissolving 5 mg of ZnO NPs in 5 ml PBS solution using sonication for 30 minutes to obtain stock solution, then serial make dilution with concentration 0.625, 0.125, 0.25, 0.5 and 1 mg/mL for both ZnO NPs samples.

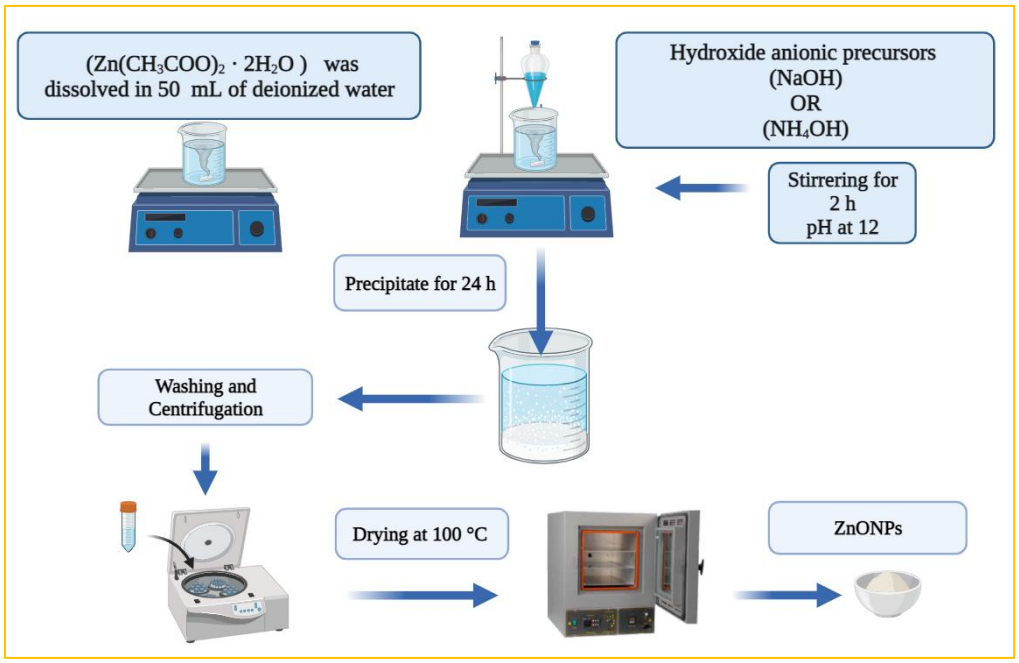

Figure (1): Diagrammatic visualization of ZnO NPs synthesis using two hydroxide anionic precursors (Sodium hydroxide and Ammonium hydroxide)

After 24 h of cell culturing, cells were washed with PBS and 100 µl of new culture media containing ZnO NPs with concentration 0.625, 0.125, 0.25, 0.5 and 1 mg/ml were added to each well and incubated at 37°C, 5% CO_2 for 24 h. Next day, standardized [3-(4, 5-dimethylthiazol-2-yl)-2, 5-diphenyltetrazolium] was used for measuring the percentage of viable cells. For preparation of MTT solution, 5 mg of MTT reagent was dissolved in PBS 5 ml under stirring for 1 h. The formed solution was then filter, sterilized and stored in dark at 4 °C **(Ahmed et al., 2023)**. For cytotoxicity measurements, the culture media was removed from cells after 24 h of treatment with ZnO NPs and cells were washed with PBS to remove debris. For conducting MTT assay, 100 µl containing (80 µl of media without serum and 20 µl of MTT solution) were added to each well and the whole plate were incubated in dark at 37°C for 3 h. Following, 100 µl of MTT stopping reagent (DMSO) was added to cells under shaking condition for 15 min in dark. Finally, the absorbance at 590 nm of each well was measured spectrophotometrically. The percentage of viable cells was normalized in respect to corresponding control and calculated using the following formula:

$$Precentage\ of\ cell\ viability(\%) = \frac{A_{sample} - A_{control}}{A_{control}}$$

Where A_{sample} is the absorption of sample and $A_{control}$ is the absorption of the control (cells without NPs).

The experiment was conducted three times, and the calculated values were expressed as the mean of the three experiments ± standard deviation.

3. Results and Discussion

3.1 Structural identification of ZnO samples using XRD

The XRD pattern of the ZnO NPs prepared by the chemical precipitation method using NH_4OH and NaOH as hydroxide anion precursors is shown in Figure (2). All the observed peaks were

appertained to ZnO wurtzite structure, which was agree with the reported card (**JCPDS Card No. 01-089-0510**) **(Thomas, 2014)**, see Table (1). The sharp diffraction peaks of the ZnO $_{(NH4OH)}$ NPs sample indicate the higher crystallinity of this sample compared with ZnO $_{(NaOH)}$ NPs. This result suggested that the change of the anionic precursor didn't alter the structure of ZnO NPs, instead, it changed the crystallinity of ZnO NPs **(Raou, 2013)**.

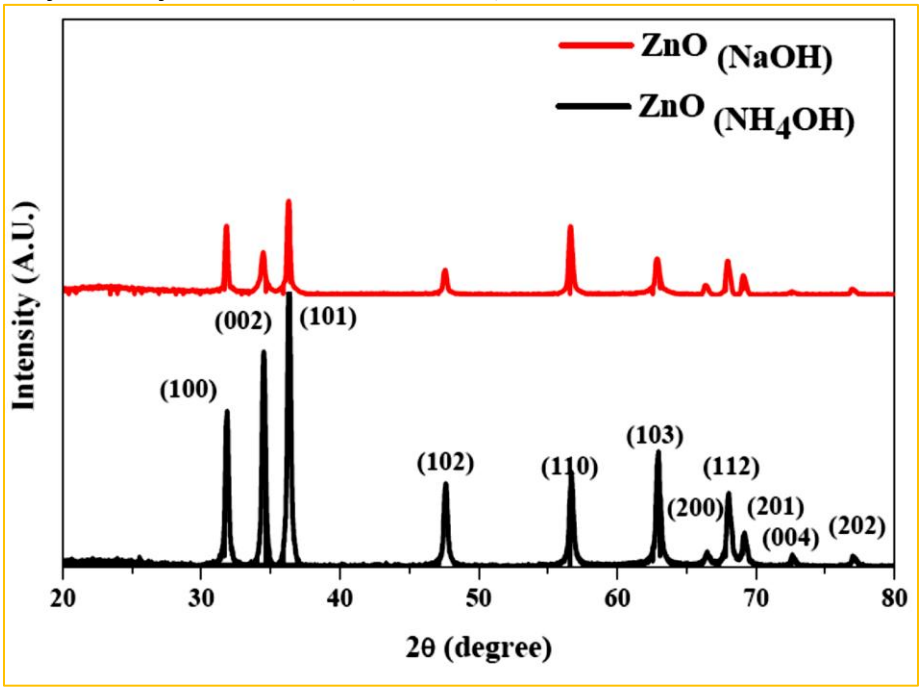

Figure (2): XRD diffraction of ZnO NPs synthesized using ammonium hydroxide and sodium hydroxide as hydroxide anion precursors.

The average crystallite size of the samples was calculated using Scherer's formula **(Alghamdi et al., 2023)**:

$$D_L = \frac{0.9\lambda}{\Gamma Cos\theta}$$

Where D_L is the average crystal size, 0.9 is a constant, λ is the wavelength of the X-ray source, θ is the diffraction angle, and Γ is the angular line broadening and represents the full width at half maximum of diffraction peaks.

For ZnO $_{(NH4OH)}$ the calculated average crystal size was 24.5± 1.5 nm, while for ZnO $_{(NaOH)}$ it was 23.044± .84 nm, see Table (1). These results indicate a small difference in the crystallite size occurs by changing the anionic procurers, which is in line with the reported results **(Amirthavalli et al., 2018; Arya et al., 2021)**. As ZnO production begins with the creation of hydrated hydroxides [(Zn $(OH)_2$ and HO-Zn groups] as precursor molecules at an earlier stage of solid material nucleation, the amount of moles of HO-must be at least twice that of Zn^{2+} **(Tokumoto et al., 2003)**.

3.2 HRTEM analysis

Figures (3) and (4) represent the HRTEM morphology with the corresponding particle size distribution of the synthesized ZnO $_{(NH4OH)}$ and ZnO $_{(NaOH)}$, respectively. With the change of the hydroxide anion precursors, a small change in the particle size was observed. The average particle size as calculated from HRTM images was 24 ± 7.1 nm and 17.8 ± 5.2 nm for ZnO $_{(NH4OH)}$ and ZnO $_{(NaOH)}$, respectively, which is in line with the obtained results from XRD. Due to the fact that the crystallite size determined by Scherer's equation does not equal the particle

size—particularly in the case of polydisperse NPs with aggregation, like ZnO NPs, where one particle often contains many crystals—these values are smaller than those derived from XRD results.

Table 1: Peak position, Interplanar spacing d_{hkl} for corresponding Miller indices (*hkl*), FWHM and the calculated particle size (D nm) from XRD data of ZnO $_{(NH4OH)}$ and ZnO $_{(NaOH)}$ NPs and JCPDS Card No. 01-089-0510.

ZnO $_{(NH4OH)}$								
Plane	2θ $_{(card)}$	d_{hkl} $_{(card)}$	I $_{(card)}$	2θ	FWHM	I	d_{hkl}	D (nm)
(100)	31.78	2.814	4085	31.8414	0.331	2160.4	2.80708	26.05732
(002)	34.42	2.603	3106	34.4952	0.338	2646.8	2.59695	25.69428
(101)	36.26	2.475	7758	36.4177	0.341	4193	2.46414	25.60519
(102)	47.54	1.911	1701	47.6139	0.376	1037.8	1.90756	24.11041
(110)	56.61	1.624	2454	56.7799	0.409	1301.5	1.61945	23.05141
(103)	62.86	1.477	2213	62.9829	0.432	1422.7	1.47405	22.51552
ZnO $_{(NaOH)}$								
Plane	2θ $_{(card)}$	d_{hkl} $_{(card)}$	I $_{(card)}$	2θ	FWHM	I	d_{hkl}	D (nm)
(100)	31.78	2.814	4085	31.7966	0.358	1560.4	2.81093	24.08941
(002)	34.42	2.603	3106	34.4532	0.367	1846.8	2.60002	23.66125
(101)	36.26	2.475	7758	36.2858	0.372	3093	2.4728	23.46256
(102)	47.54	1.911	1701	47.5769	0.396	702.17	1.90896	22.88946
(110)	56.61	1.624	2454	56.627	0.425	975.35	1.62346	22.16763
(103)	62.86	1.477	2213	62.8907	0.442	843.74	1.47599	21.99528

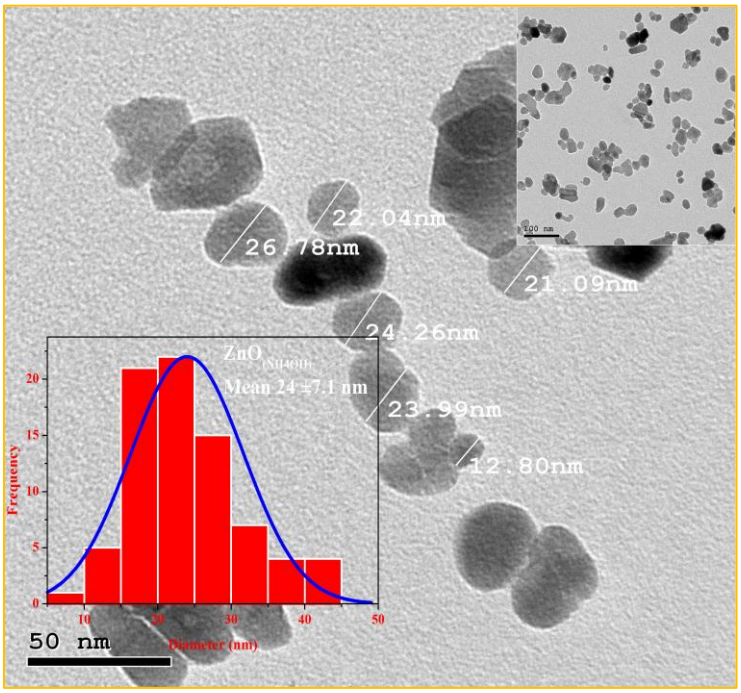

Figure (3): HTEM image of ZnO $_{(NH4OH)}$ with the corresponding particle size distribution; the main image with scale bar 50 nm and the image in the right corner with scale bar 100 nm.

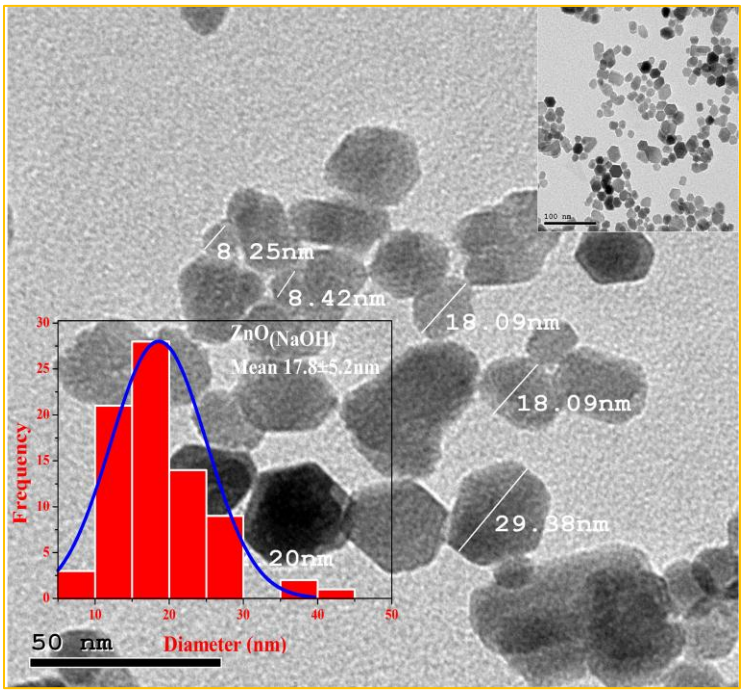

Figure (4): HTEM image of ZnO $_{(NaOH)}$ with the corresponding particle size distribution; the main image with a scale bar 50 nm and the image in the right corner with a scale bar 100 nm.

3.4 UV-visible spectroscopy

The optical activity of ZnO NPs synthesized with different hydroxide anion precursors was investigated using UV-visible spectroscopy. The absorption spectra of both samples reflect the absorption edge at 370 and 365 nm for ZnO $_{(NH4OH)}$ and ZnO $_{(NaOH)}$, respectively, Figure (5). The observed blue shift in the absorption edge of both samples compared with the reported value for ZnO (376 nm) was mainly due to the change of crystal size, which is confirmed by the structural analysis **(Almeida et al., 2021; Amirthavalli et al., 2018)**. Furthermore, neither sample's spectra showed any new peaks, indicating that they were both pure. A number of variables, including the band gap, oxygen insufficiency, size, shape, surface chemistry, and impurity centers, affect absorption. One particularly noteworthy characteristic of ZnO that attracted interest in biomedical applications was its high capacity for UV absorption **(Selvanathan et al., 2022)**.

The band gap of the investigated ZnO NPs was measured with the well-known Tauc equation **(Almeida et al., 2021; Kahouli et al., 2015)**:

$$(\alpha h\nu) = A(h\nu - E_g)^n$$

where α is the absorption factor, A is a constant, $h\nu$ is the photon energy, E_g is the optical band gap energy and n is a number represent the allowed transition n=1/2 or 2 for direct transition and indirect transitions, respectively. The band gap can be determined graphically from the liner fitting of the graph of $(\alpha h\nu)^2$ verse $h\nu$, as shown in Figure (6). The calculated bandgap was 3.19 and 3.22 e.v for ZnO $_{(NH4OH)}$ and ZnO $_{(NaOH)}$, respectively.

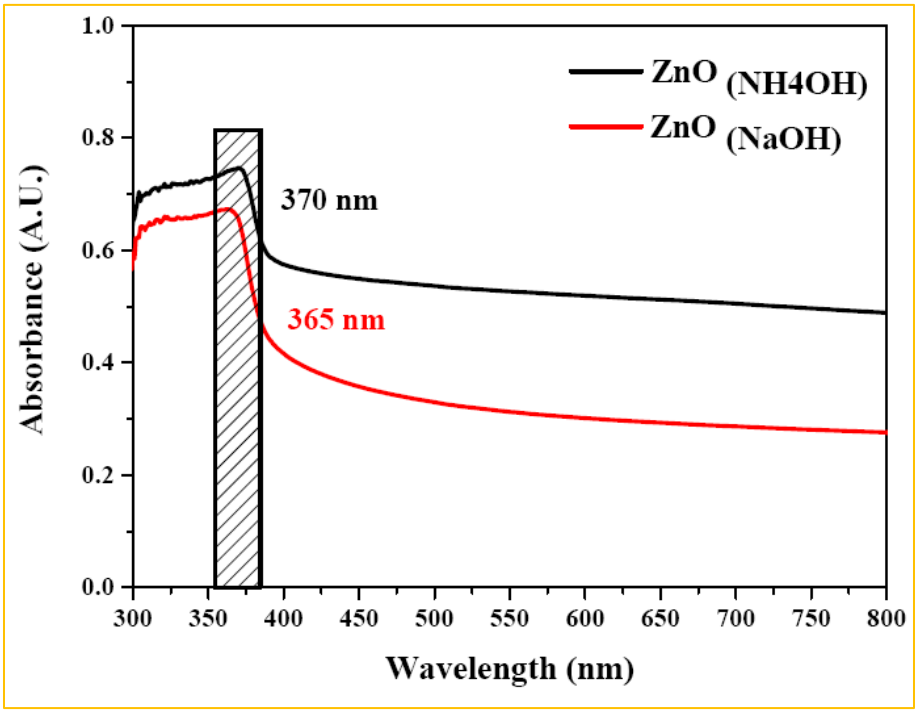

Figure (5): Absorption Spectra of ZnO $_{(NH4OH)}$ and ZnO $_{(NaOH)}$

According to structural analysis, which is also consistent with the published results, the tiny difference in the optical bandgap of both samples relative to the bulk ZnO may be caused by variations in particle size. The optical bandgap increased with the decrease in the particle size **(Amirthavalli et al., 2018; Fonoberov & Balandin, 2007; Zno, 2009)**.

4.3 Anticancer activity

One of the most challenges of NPs as anticancer agents is the selectivity of cancer cells **(Bai et al., 2017)**. ZnO NPs are characterized by a high selectivity to cancer cells compared to normal cells. The presence of anionic phospholipids with a high concentration promotes the electrostatic attraction of ZnO NPs with cancer cells, which facilitates selective targeting. Once this selective targeting occurs the cellular uptake initiates resulting in cellular distraction and death **(Anjum et al., 2021; Raffa et al., 2011)**. The reported mechanism of ZnO NPs cytotoxicity started with the cellular uptake then ZnO NPs dissolved to Zn ions, which initiate the production of reactive oxygen species (ROS). Due to the high selectivity of ZnO NPs to cancer cells, the number of generated ROS in cancer cells is higher than that in normal cells **(Ahamed et al., 2012; Levy et al., 2017)**. Particle size, shape and surface chemistry are key parameters in the anticancer activity of NPs. All the parameters are related to the synthesis methods and functionalization of NPs **(Gomathi et al., 2021; Gupta et al., 2013)**. In our proposed work we focus on the change of hydroxide anionic precursors on the physiochemical and anticancer activity of ZnO NPs.

MTT assay was used to assess the toxic effect of the synthesized ZnO NPs samples against MCF-7 cells, Figure (7). A gradual decrease in the MCF-7 cell viability was observed as the concentration of both samples ZnO NPs increased compared to control cells (cells without NPs), which confirm the production of ROS. The calculated IC_{50} was 0.66 and 0.86 mg/mL for ZnO $_{(NaOH)}$ and ZnO $_{(NH4OH)}$ samples respectively. Figures (8) and (9) show the microscopic images of cells under investigation after exposure to ZnO $_{(NaOH)}$ and ZnO $_{(NH4OH)}$, respectively with two concentrations (0.0625 and 1 mg/mL). At low concentration (0.0625 ml/mL) cells have the

normal shape and morphology, while at high concentration (1 mg/mL) cells tend to shrink due to cell apoptosis **(Król et al., 2017; Rafique et al., 2023)**.

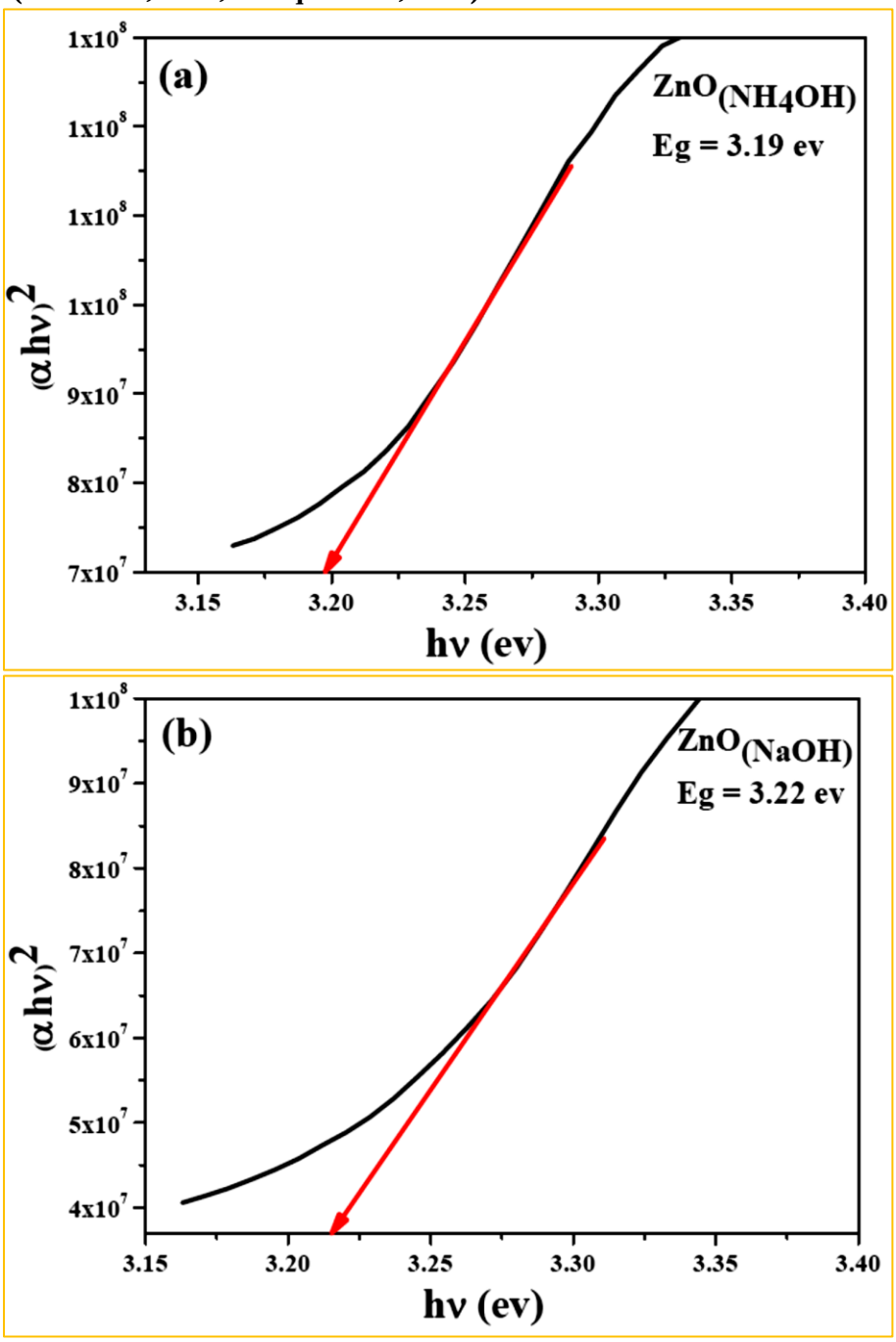

Figure (6): Optical bandgap calculation using Tauc equation for (a) ZnO $_{(NH4OH)}$ and (b) ZnO $_{(NaOH)}$

As the structural study reveals, the change of the hydroxide anionic precursor was confirmed to cause changes in the physicochemical properties of ZnO NPs. Herein this context, the MCF7 cell viability of the ZnO $_{(NaOH)}$ sample showed a higher decrease compared with that of the ZnO $_{(NH4OH)}$ sample. This change in the cytotoxicity profile of both samples may be attributed to the change in the particle size. The smaller particle size enhances the penetration of ZnO NPs into the

cell wall, which in turn will affect the number of generated ROS and increase the number of dead cells **(Baranowska-wójcik, 2021; Gomathi et al., 2021)**.

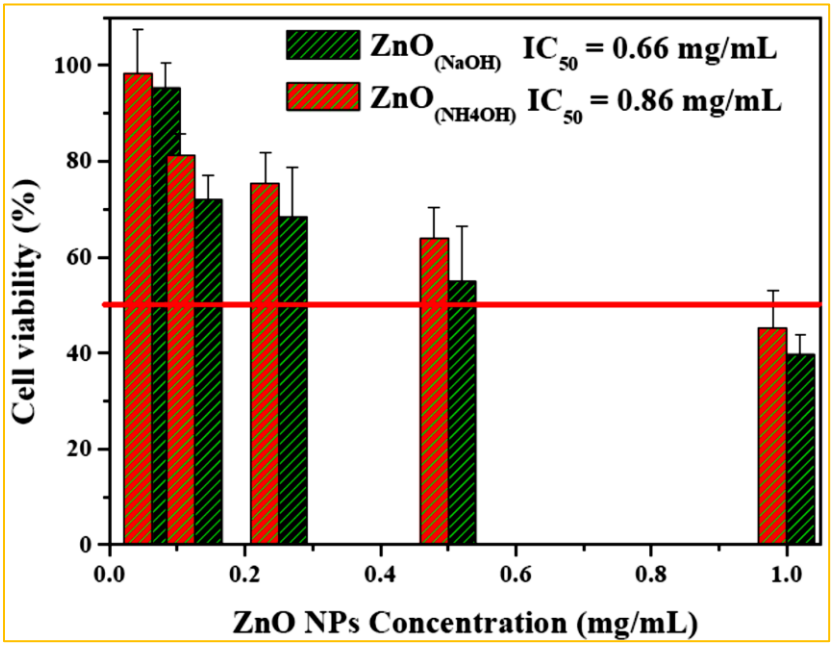

Figure (7): percentage of viable MCF-7 cells normalized to control after treatment with different concentrations of ZnO $_{(NH4OH)}$ and ZnO $_{(NaOH)}$ NPs for 24 h.

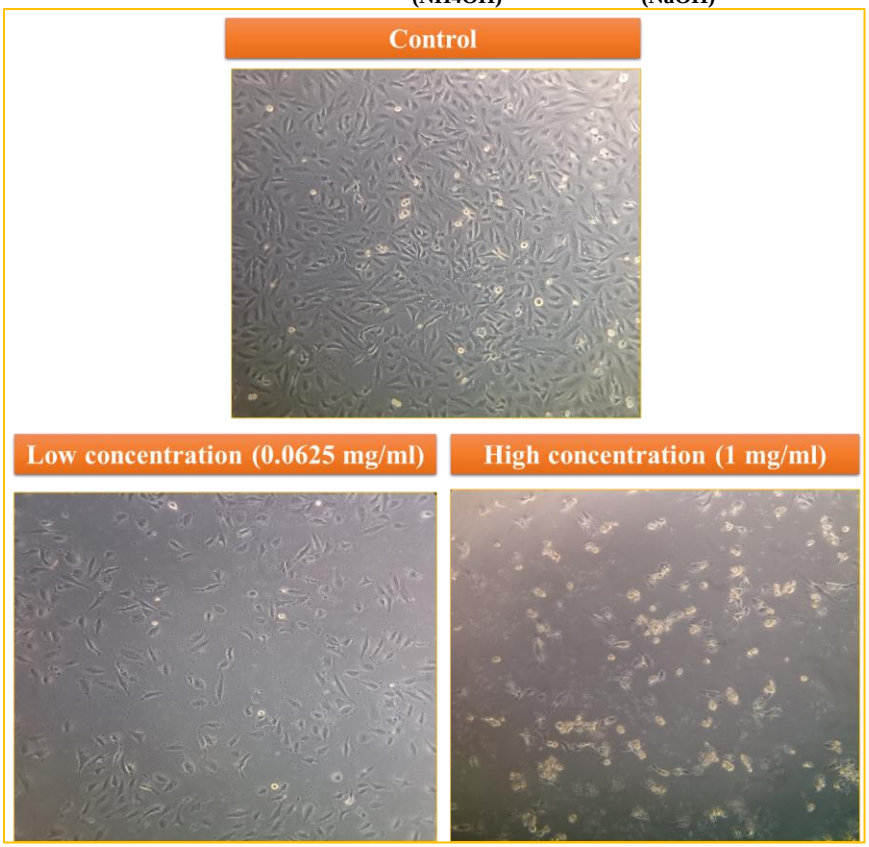

Figure (8): MCF-7 control cells and cells treated ZnO $_{(NaOH)}$ NPs at varying concentrations for 24 h under a microscope (1 and 0.0625 mg/ml).

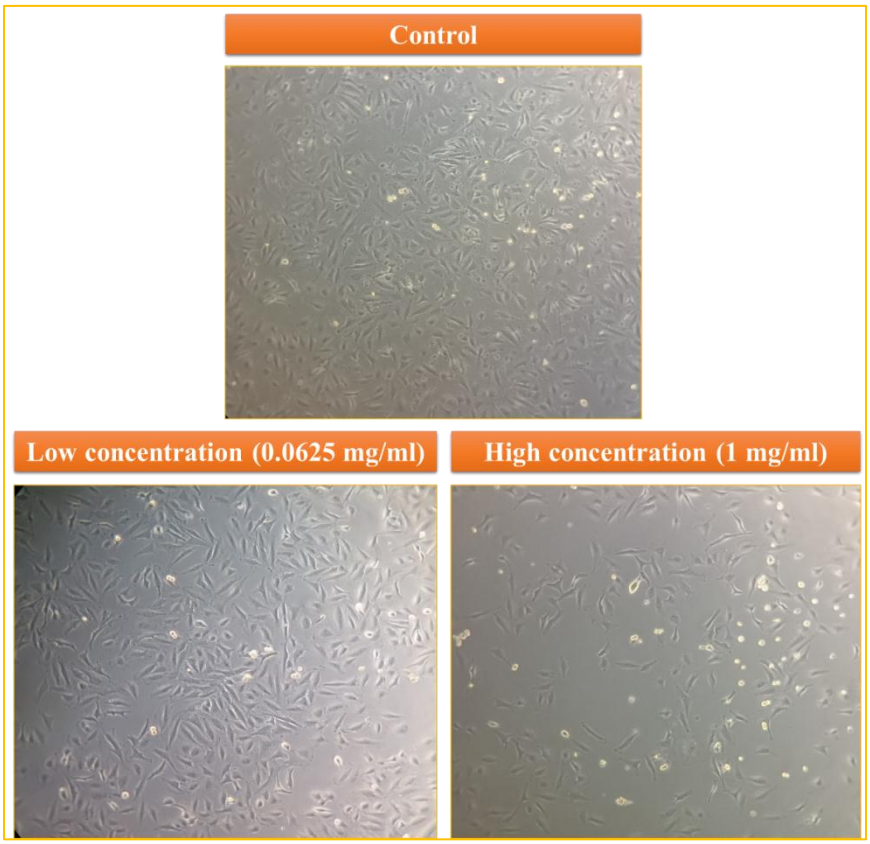

Figure (9): MCF-7 control cells and cells treated ZnO $_{(Na4OH)}$ NPs at varying concentrations for 24 h under a microscope (1 and 0.0625 mg/ml).

4. Conclusion

ZnO NPs were successfully synthesized from two different anionic precursors (Sodium hydroxide and Ammonium hydroxide) using the chemical precipitation method. The structural analysis reveals the successful formation of ZnO NPs in both samples under investigation as the fingerprint peaks of ZnO NPs appeared in XRD and UV-vis spectra of both samples. Cytotoxicity measurements reflect a higher decrease in MCF-7 cell viability after exposure to ZnO $_{(NaOH)}$ compared with that of the ZnO $_{(NH4OH)}$ sample. This change in the cytotoxicity profile of both samples may be attributed to the change in the particle size. The smaller particle size enhances the penetration of ZnO NPs into the cell wall, which in turn will affect the number of generated ROS and increase the number of dead cells.

Acknowledgements

Not applicable.

Authors' contributions

Eman Hussein did the experimental part and Alaa Hassan Said analyzed the data and wrote the original manuscript. Gharib H. Taha and Kh. Ebenlwaled revised the original manuscript. All authors read and approved the final manuscript.

Availability of data and materials

All the data used to support the findings of this study are included in the article. Other data are available from the corresponding author upon request

Competing interests

The authors declare that they have no competing interests.

References

Ahamed, M., Javed Akhtar, Kumar, Khan, M., Ahmad, & Alrokayan. (2012). Zinc oxide nanoparticles selectively induce apoptosis in human cancer cells through reactive oxygen species. *International Journal of Nanomedicine*, 845. https://doi.org/10.2147/IJN.S29129

Ahmadi Shadmehri, A., & Namvar, F. (2020). A Review on Green Synthesis, Cytotoxicity Mechanism and Antibacterial Activity of Zno-NPs. *Journal of Research in Applied and Basic Medical Sciences*, *6*(1), 23–31.

Ahmed, N. K., Abbady, A., Elhassan, Y. A., & Said, A. H. (2023). Green Synthesized Titanium Dioxide Nanoparticle from Aloe Vera Extract as a Promising Candidate for Radiosensitization Applications. *BioNanoScience*, *13*(2), 730–743. https://doi.org/10.1007/s12668-023-01085-2

Alghamdi, R. A., Al-Zahrani, M. H., Altarjami, L. R., Al Abdulmonem, W., Samir, N., Said, A., Shami, A. A., Mohamed, W. S., & Ezzeldien, M. (2023). Biogenic Zinc oxide nanoparticles from Celosia argentea: toward improved antioxidant, antibacterial, and anticancer activities. *Frontiers in Bioengineering and Biotechnology*, *11*. https://doi.org/10.3389/fbioe.2023.1283898

Almeida, W. L. De, Ferreira, N. S., Rodembusch, F. S., & Sousa, D. (2021). *Study of structural and optical properties of ZnO nanoparticles synthesized by an eco-friendly tapioca-assisted route*. *258*(October 2020). https://doi.org/10.1016/j.matchemphys.2020.123926

Amirthavalli, C., Manikandan, A., & Prince, A. A. M. (2018). E ff ect of zinc precursor ratio on morphology and luminescent properties of ZnO nanoparticles synthesized in CTAB medium. *Ceramics International*, *44*(13), 15290–15297. https://doi.org/10.1016/j.ceramint.2018.05.173

Anjum, S., Hashim, M., Malik, S. A., Khan, M., Lorenzo, J. M., Abbasi, B. H., & Hano, C. (2021). Recent advances in zinc oxide nanoparticles (Zno nps) for cancer diagnosis, target drug delivery, and treatment. *Cancers*, *13*(18). https://doi.org/10.3390/cancers13184570

Arya, S., Mahajan, P., Mahajan, S., Khosla, A., Datt, R., Gupta, V., Young, S.-J., & Oruganti, S. K. (2021). Review—Influence of Processing Parameters to Control Morphology and Optical Properties of Sol-Gel Synthesized ZnO Nanoparticles. *ECS Journal of Solid-State Science and Technology*, *10*(2), 023002. https://doi.org/10.1149/2162-8777/abe095

Bai, D. P., Zhang, X. F., Zhang, G. L., Huang, Y. F., & Gurunathan, S. (2017). Zinc oxide nanoparticles induce apoptosis and autophagy in human ovarian cancer cells. *International Journal of Nanomedicine*, *12*, 6521–6535. https://doi.org/10.2147/IJN.S140071

Baranowska-wójcik, E. (2021). *Factors Conditioning the Potential Effects TiO_2 NPs Exposure on Human Microbiota: a Mini-Review*. 4458–4465.

Barhoum, A., Rahier, H., Benelmekki, M., & Assche, G. Van. (2018). Recent trends in nanostructured particles: synthesis, functionalization, and applications. *Fundam Nanopart*, 605–639. https://doi.org/10.1016/b978-0-323-51255-8.00024-0

Bisht, G., Rayamajhi, S., Article, R., Bisht, G., & Rayamajhi, S. (2016). ZnO Nanoparticles: A Promising Anticancer Agent. *Nanobiomedicine*, *3*, 9. https://doi.org/10.5772/63437

Chung, I., Rahuman, A. A., Marimuthu, S., Kirthi, A. V., Anbarasan, K., & Rajakumar, G. (2015). *An Investigation of the Cytotoxicity and Caspase-Mediated Apoptotic Effect of Green Synthesized Zinc*

Oxide Nanoparticles Using Eclipta prostrata on Human Liver Carcinoma Cells. 1317–1330. https://doi.org/10.3390/nano5031317

Fonoberov, V., & Balandin, A. A. (2007). *Micro-Raman spectroscopic characterization ZnO quantum dots, nanocrystals , and ... March*. https://doi.org/10.1117/12.713648

Fröhlich, E. (2012). The role of surface charge in cellular uptake and cytotoxicity of medical nanoparticles. *International Journal of Nanomedicine*, *7*, 5577–5591. https://doi.org/10.2147/IJN.S36111

Gomathi, R., Suhana, H., & Paradesi, D. (2021). Characterization Study of Cytotoxicity of Green Synthesized ZnO Nanoparticles Loaded with Anti-Cancer Doxorubicin Drug. *ChemistrySelect*, *6*(18), 4533–4538. https://doi.org/10.1002/slct.202100358

Gupta, A., Avci, P., Sadasivam, M., Chandran, R., Parizotto, N., Vecchio, D., de Melo, W. C. M. A., Dai, T., Chiang, L. Y., & Hamblin, M. R. (2013). Shining light on nanotechnology to help repair and regeneration. *Biotechnology Advances*, *31*(5), 607–631. https://doi.org/10.1016/j.biotechadv.2012.08.003

Harun, K., Mansor, N., Ahmad, Z. A., & Mohamad, A. A. (2016). Electronic properties of ZnONPs synthesized by sol–gel method: a LDA+ U calculation and experimental study. *Procedia Chem*, *19*, 125–132. https://doi.org/10.1016/j.proche.2016.03.125

Ibrahim, A. H., & Shash, E. (2022). General Oncology Care in Egypt. In *Cancer in the Arab World* (pp. 41–61). Springer Singapore. https://doi.org/10.1007/978-981-16-7945-2_4

Kahouli, M., Barhoumi, A., Bouzid, A., Al-hajry, A., & Guermazi, S. (2015). Superlattices and Microstructures Structural and optical properties of ZnO nanoparticles prepared by direct precipitation method. *Superlattices and Microstructures*, *85*, 7–23. https://doi.org/10.1016/j.spmi.2015.05.007

Koutu, V., Shastri, L., & Malik, M. M. (2016). *Effect of NaOH concentration on optical properties of zinc oxide nanoparticles*. *34*(4), 819–827. https://doi.org/10.1515/msp-2016-0119

Król, A., Pomastowski, P., Ra, K., & Buszewski, B. (2017). *Zinc oxide nanoparticles: Synthesis , antiseptic activity and toxicity mechanism*. *249*, 37–52. https://doi.org/10.1016/j.cis.2017.07.033

Levy, J. M. M., Towers, C. G., & Thorburn, A. (2017). Targeting autophagy in cancer. *Nature Publishing Group*, *17*(9), 528–542. https://doi.org/10.1038/nrc.2017.53

Limón- rocha, I., Guzmán- González, C. A., Anaya- esparza, L. M., Romero- toledo, R., Rico, J. L., González- vargas, O. A., & Pérez- larios, A. (2022). Effect of the Precursor on the Synthesis of ZnO and Its Photocatalytic Activity. *Inorganics*, *10*(2). https://doi.org/10.3390/inorganics10020016

Loganathan, S., Shivakumar, M. S., Karthi, S., Nathan, S. S., & Selvam, K. (2021). Metal oxide nanoparticle synthesis (ZnO-NPs) of Knoxia sumatrensis (Retz.) DC. Aqueous leaf extract and It's evaluation of their antioxidant, anti-proliferative and larvicidal activities. *Toxicology Reports*, *8*, 64–72. https://doi.org/10.1016/j.toxrep.2020.12.018

Nam, J., Won, N., Bang, J., Jin, H., Park, J., Jung, S., Jung, S., Park, Y., & Kim, S. (2013). Surface engineering of inorganic nanoparticles for imaging and therapy. *Advanced Drug Delivery Reviews*, *65*(5), 622–648. https://doi.org/10.1016/j.addr.2012.08.015

Raffa, V., Riggio, C., Vittorio, O., Iorio, M. C., Vanacore, R., Pietrabissa, A., & Cuschieri, A. (2011). *Zinc oxide nanoparticles as selective killers of proliferating cells*. 1129–1140. https://doi.org/10.2147/IJN.S16581

Rafique, S., Bashir, S., Akram, R., Jawaid, S., Bashir, M., Aftab, A., Attique, A., & Awan, S. U. (2023). In vitro anticancer activity and comparative green synthesis of ZnO/Ag nanoparticles by moringa oleifera, mentha piperita, and citrus lemon. *Ceramics International*, *49*(4), 5613–5620. https://doi.org/10.1016/j.ceramint.2022.10.163

Raou, D. (2013). *Synthesis and microstructural properties of ZnO nanoparticles prepared by precipitation method*. *50*, 932–937. https://doi.org/10.1016/j.renene.2012.08.076

Rasmussen, J. W., Martinez, E., Louka, P., & Wingett, D. G. (2010). Zinc oxide nanoparticles for selective destruction of tumor cells and potential for drug delivery applications. In *Expert Opinion on Drug Delivery* (Vol. 7, Issue 9, pp. 1063–1077). https://doi.org/10.1517/17425247.2010.502560

Schumm, M. (2008). *ZnO-based semiconductors studied by Raman spectroscopy: semimagnetic alloying, doping , and nanostructures*.

Selvakumari, D., Deepa, R., Mahalakshmi, V., Subhashini, P., & Lakshminarayan, N. (2015). Anti-cancer activity of zno nanoparticles on MCF7 (breast cancer cell) and A549 (lung cancer cell). *ARPN Journal of Engineering and Applied Sciences*, *10*(12), 5418–5421.

Selvanathan, V., Aminuzzaman, M., Xian, L., Foo, Y., Seong, E., Cheah, G., Hsuan, M., Tey, L., Arullappan, S., & Algethami, N. (2022). Synthesis, characterization, and preliminary in vitro antibacterial evaluation of ZnO nanoparticles derived from soursop (Annona muricata L .) leaf extract as a green reducing agent. *Journal of Materials Research and Technology*, *20*, 2931–2941. https://doi.org/10.1016/j.jmrt.2022.08.028

Siegel, R. L., Miller, K. D., Fuchs, H. E., & Jemal, A. (2021). Cancer Statistics, 2021. *CA: A Cancer Journal for Clinicians*, *71*(1), 7–33. https://doi.org/10.3322/caac.21654

Thomas, P. B. S. (2014). *Estimation of lattice strain in ZnO nanoparticles: X-ray peak profile analysis*. 123–134. https://doi.org/10.1007/s40094-014-0141-9

Tokumoto, M. S., Briois, V., Santilli, C. V, & Pulcinelli, S. H. (2003). *Preparation of ZnO Nanoparticles: Structural Study*. 547–551.

Zno, M. (2009). *Analysis of Raman modes in Mn-doped ZnO nanocrystals*. *2332*(10), 2329–2332. https://doi.org/10.1002/pssb.200945192